

Scaling Laws and Critical Properties for *FCC* and *HCP* Metals.

Caroline Desgranges, Leanna Widhalm, and Jerome Delhommelle*

Department of Chemistry, University of North Dakota, Grand Forks, ND 58202, USA

(Phone: 701-777-2495)

E-mail: jerome.delhommelle@und.edu

*To whom correspondence should be addressed

Abstract

The determination of the critical parameters of metals has remained particularly challenging both experimentally, because of the very large temperatures involved, and theoretically, because of the many-body interactions that take place in metals. Moreover, experiments have shown that these systems exhibit an unusually strong asymmetry of their binodal. Recent theoretical work has led to new similarity laws, based on the calculation of the Zeno line and of the underlying Boyle parameters, which provided results for the critical properties of atomic and molecular systems in excellent agreement with experiments. Using the recently developed Expanded Wang-Landau (EWL) simulation method, we evaluate the grand-canonical partition function, over a wide range of conditions, for 11 *FCC* and *HCP* metals (*Ag, Al, Au, Be, Cu, Ir, Ni, Pb, Pd, Pt* and *Rh*), modeled with a many-body interaction potential. This allows us to calculate the binodal, Zeno line, Boyle parameters and, in turn, obtain the critical properties for these systems. We also propose two scaling laws for the enthalpy and entropy of vaporization, and identify critical exponents of 0.4 and 1.22 for these two laws, respectively.

Introduction

The determination of the critical properties often relies on the extrapolation^{1–8} of low temperature results using e.g., for the critical density, the law of rectilinear diameter.⁹ This law is based on the observation of the linearity of the diameter ρ_m of the liquid-vapor coexistence curve as a function of temperature, with $\rho_m = 0.5(\rho_l + \rho_v)$ where ρ_l and ρ_v are the liquid density and vapor density at coexistence, respectively. Although this law seems to hold for a wide range of substances,^{10,11} there have been exceptions^{12–14} most notably in the case of metals.^{15–17} For instance, for alkali metals like *Cs* and *Rb*, experiments showed that the two branches of the coexistence curves were strongly asymmetric and the law of rectilinear diameter was found to break down over a large temperature range.¹⁵ The exceptional nature of metals was attributed to the existence of many-body effects in these systems,¹⁶ which have been shown to play a major role close to the critical region.¹⁸

The knowledge of the critical properties of metals is of key importance for many applications at the nanoscale^{1,19} and for high temperature technologies,¹⁷ e. g. in aerospace and in the nuclear industry. However, there is generally a lack of experimental data on metallic systems. This is due to the large temperatures involved in the determination of the critical parameters of metals (the liquid range of metals can cover temperatures which may go above 10000 K¹⁷). These are particularly challenging to investigate and require special experimental techniques like the "exploding-wire" technique.^{20,21} As a result, the extrapolations from the experimental data exhibit large variations.^{17,22–24} For instance, estimates for the critical temperature of *Al* vary from around $T_c = 5500\text{ K}$ to $T_c = 9600\text{ K}$.²⁵ Similarly for *Cu*, the estimated critical temperatures range from 5100 K to 8900 K.^{26,27} To bridge this gap in knowledge, recent work has led to the determination of the critical properties from low temperature liquid data. These studies either used a power series law for the diameter¹⁷ or a new symmetrized equation for the vapor liquid coexistence curve.^{28–35}

The aim of this work is to use molecular simulation to determine the critical properties of a series of *FCC* and *HCP* metals modeled with a many-body force field known as the quantum-corrected Sutton-Chen potential.³⁶ This model was shown to accurately model the properties of liquid metals,^{36–44} as well as the boiling points of metals⁴⁵ and the vapor-liquid equilibrium properties of *Cu*.^{46,47} To determine the vapor-liquid properties, as well as the locus of the Zeno line, we use the recently developed Expanded Wang-Landau simulation method.^{48–51} This method leads to an accurate determination of the grand-canonical partition function of a system, and in turn, to all thermodynamic properties, including the vapor and liquid densities at coexistence and the compressibility factor. This allows us to determine the Zeno line, the Boyle parameters and the critical point for all metallic systems studied in this work.

The paper is organized as follows. In the next section, we present the simulation methods as well as the many-body force field used in this work. We show the results obtained for 11 *FCC* and *HCP* metals and explain how we determine the critical properties of these systems. We then discuss and compare our results to those obtained by extrapolating experimental data at low temperature. We finally draw the main conclusions from this work in the last section.

Simulation methods

The fluid properties at coexistence are determined using the recently developed Expanded Wang-Landau simulations (EWL).^{48–51} We give here an outline of the method. The EWL simulation method relies on a combination of a Wang-Landau sampling scheme^{46,47,52–60} with an expanded ensemble approach^{61–73} to provide an accurate value of the grand-canonical partition function for a given system. The use of a Wang-Landau sampling allows to determine iteratively the biasing function (hence the partition function), while the use of an expanded ensemble approach, which consists in dividing the insertion/deletion of an atom into M stages, ensures that the grand-canonical ensemble is accurately sampled over the whole range of conditions. This is especially key for high density liquids⁴⁸ like liquid metals. The output from the simulation are the grand-canonical partition function $\Theta(\mu, V, T)$ and the $Q(N, V, T)$ function which are related as follows:

$$\Theta(\mu, V, T) = \sum_{N=0}^{\infty} Q(N, V, T) \exp(\beta\mu N) \quad (1)$$

with $Q(N, V, T)$ defined as

$$Q(N, V, T) = \frac{V^N}{N! \Lambda^{3N}} \int \exp(-\beta U(\Gamma)) d\Gamma \quad (2)$$

where μ denotes the chemical potential, V the volume, T the temperature, N the number of atoms in the system, Λ the De Broglie wavelength, U is the potential energy of the system at a given point Γ of the configuration space.

Once the partition function is known, all thermodynamic properties of the system can be calculated through the statistical mechanics formalism⁷⁴ and the number distribution $p(N)$ can be calculated as:

$$p(N) = \frac{Q(N, V, T) \exp(\beta\mu N)}{\Theta(\mu, V, T)} \quad (3)$$

This allows to determine the densities at coexistence as well as the other thermodynamic prop-

erties at coexistence,^{48–51} including pressure P , enthalpies H_{liq} and H_{vap} as well as entropies S_{liq} and S_{vap} . From there, the location of the Zeno line, i.e. the points for which the compressibility factor $Z = PV/RT = 1$ can be readily determined.

The many-body interactions in metals are often taken into account using embedded-atom potentials (EAM).^{75–78} EAM potentials are density-dependent potentials that were initially introduced to model the properties of the solid phases of metals. In this work, we use the quantum-corrected Sutton-Chen³⁶ embedded atoms (qSC-EAM) potential. The qSC-EAM potential has been shown to accurately describe thermodynamic properties of liquid metals,^{36–44} as well as the boiling points of metals⁴⁵ and the vapor-liquid equilibrium properties of Copper.^{46,47} In the qSC-EAM potential, the potential energy U of a system containing N atoms is written as the sum of a contribution of two-body term and a contribution of a many-body term

$$U = \frac{1}{2} \sum_{i=1}^N \sum_{j \neq i} \varepsilon \left(\frac{a}{r_{ij}} \right)^n - \varepsilon C \sum_{i=1}^N \sqrt{\rho_i} \quad (4)$$

in which r_{ij} is the distance between two atoms i and j and the density term ρ_i is given by

$$\rho_i = \sum_{j \neq i} \left(\frac{a}{r_{ij}} \right)^m \quad (5)$$

We use the parameters of Luo *et al.*³⁶ for the 11 *FCC* and *HCP* metals (*Ag, Al, Au, Be, Cu, Ir, Ni, Pb, Pd, Pt* and *Rh*) studied in this work. The interaction between a fractional atom and a full atom is given by Eqs. 4 and 5 using the scaled parameters $a_l = a(l/M)^{1/4}$ instead of a and $C_l = C(l/M)^{1/3}$ instead of C where l is the current stage value of the fractional particle ($0 < l < M - 1$). Fig. 1 shows the dependence of the potential for the full-fractional interaction as a function of the stage value for the fractional particle. From a practical standpoint, EWL simulations are carried out within the framework of Monte Carlo (MC) simulations. To sample the configurations of the system, we perform MC steps corresponding to the translation of a single atom (75% of the MC steps) or to a change in (N, l) for the system (25% of the MC steps). The EWL method yields accurate results, with error bars⁴⁸ typically of the order of 0.1% for the density and of 0.02 % for

the enthalpy and entropy. The technical details regarding the Wang-Landau scheme are exactly the same as previously described,^{48,49} with the final value of the convergence factor set to $f = 10^{-8}$ and a number of intermediate stages set to $M = 100$.

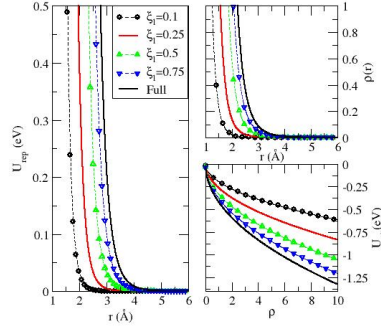


Figure 1: Interaction between a fractional atom and a full atom. Results are shown for different values of $\xi_l = l/M$ for the 2-body contribution (left), the local density (top right) and the many-body contribution (bottom right).

Results and discussion

We start by presenting, on the example of Ir , the results obtained using the EWL approach. Fig. 2 shows the density distributions $p(\rho = N/V)$ obtained at coexistence for three temperatures, $T = 4400\text{ K}$, $T = 4800\text{ K}$ and $T = 5200\text{ K}$. In the left panel of Fig. 2, we plot the density distributions for the vapor phase while the right panel of Fig. 2 shows the density distribution for the liquid phase. These plots exhibit the expected behavior for the distributions, i.e. a shift towards the higher densities for the vapor peak as temperature increases and a shift towards the lower densities for the liquid peak as T increases.

We now turn to the density distributions obtained for Ir along the Zeno line. We recall that this is obtained, for each temperature, by identifying the value of the chemical potential that ensures that the ratio $Z = PV/RT$ is equal to 1. The density distribution corresponding to the chemical potential so obtained is plotted, for each temperature, in Fig. 3. We see that in this case we obtain a

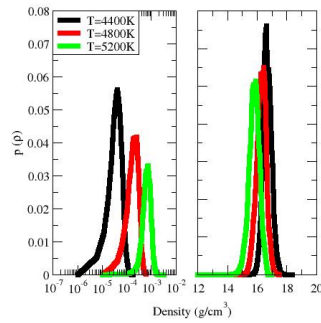


Figure 2: *Ir*: density distribution $p(\rho)$ for the vapor (left) and for the liquid (right) along the coexistence line.

single peak (corresponding to a single phase system) which gets shifted towards the lower densities as T increases.

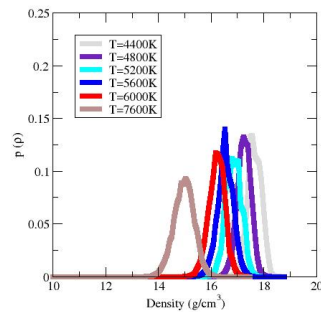


Figure 3: *Ir*: density distribution $p(\rho)$ along the Zeno line.

The phase diagram in the $T - \rho$ plane, as well as the location of the Zeno line in that plane can be readily determined from the density distributions. The complete results for *Ir* are indicated in Fig. 4 with the densities at coexistence and the locus of the Zeno line. The results confirm that the Zeno line is straight over the range of liquid densities considered in this work.⁷⁹ This plot also shows the Boyle parameters for *Ir* as well as the critical point. The Boyle parameters are determined by performing a linear fit to the EWL results along the Zeno line. The critical

parameters are then determined from the EWL results as follows. First, the critical temperature is extrapolated from the densities of the two coexisting phases through the following fit:

$$\rho_l - \rho_v = A(T_c - T)^{0.326} \quad (6)$$

where A and T_c are two fitting parameters, ρ_l and ρ_v are the densities for the liquid and vapor phases at a given temperature T and the 3D-Ising critical exponent, adjusted for real substances, of 0.326 is used.

Second, the critical density ρ_c is obtained using the following similarly relation:²⁹

$$\frac{T_c}{T_B} + \frac{\rho_c}{\rho_B} = S_1 \quad (7)$$

where T_c is the critical temperature determined using the previous equation, T_B and ρ_B are the Boyle temperature and density, S_1 is a parameter equal to 0.67 (as established by Apfelbaum *et al.* for several systems,⁸⁰ including *Be*, *Cu* and *Al*), and ρ_c is a fitting parameter. Using this similarity law alleviates the need to use the law of rectilinear diameter, that has been shown to break down for metals,¹⁵ to determine the critical density of metals

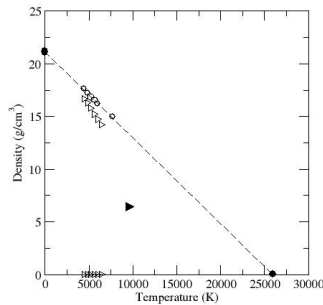


Figure 4: *Ir*: EWL results for the vapor-liquid equilibrium curve (open triangles) and for the Zeno line (open circles). The critical point is shown as a filled triangle while the Boyle parameters are shown with filled circles.

We apply the same approach to all 11 *FCC* and *HCP* metals considered in this work. Table 1

summarizes the results obtained in this work both for the Boyle and critical parameters. In addition to the critical temperatures and densities, we also provide an estimate for the critical pressure. The critical pressure is obtained by fitting an Antoine law to the results obtained for the pressure. The fit to the Antoine law is carried out according to:

$$\log_{10} P = A + \frac{B}{T + C} \quad (8)$$

where A , B and C are fitting parameters and P is the vapor pressure for a given temperature T . The critical pressure is calculated from this law using the value for the critical temperature previously obtained from Eq. 6.

Table 1: Boyle and critical parameters obtained in this work for FCC and HCP metals.

	T_B (K)	ρ_B (g/cm ³)	T_c (K)	ρ_c (g/cm ³)	P_c (MPa)
<i>Ag</i>	11488	9.97	4260	2.98	34.3
<i>Al</i>	15316	2.56	5412	0.81	37.9
<i>Au</i>	12627	18.02	4286	5.96	18.6
<i>Be</i>	12534	1.71	4623	0.52	88.6
<i>Cu</i>	15688	8.36	5430	3.33	57.8
<i>Ir</i>	25974	21.15	9484	6.45	91.7
<i>Ni</i>	19502	8.35	6700	2.72	62.1
<i>Pb</i>	8287	10.16	2663	3.54	7.2
<i>Pd</i>	14888	11.29	5444	3.44	50.1
<i>Pt</i>	21472	20.00	7375	6.53	44.5
<i>Rh</i>	21691	11.72	8106	3.47	62.1

We first discuss the results obtained for *Be*. We start by comparing the EWL results for the Boyle parameters to those obtained in previous work by Apfelbaum²⁹ using an effective ion-ion potential to model liquid *Be*. We obtain a very good agreement for the Boyle density between the EWL results on the qSC-EAM potential (1.714 g/cm³) and the previous estimate (1.697 g/cm³), and a reasonable agreement for the Boyle temperature with a EWL value of 12534 K compared to 10500 K. The critical temperature (see Table 2) we estimate from our EWL results ($T_c = 4623$ K) is in reasonable agreement with the predicted value of 5400 K by Apfelbaum,²⁹ obtained by analyzing the low temperature liquid data for *Be*. Using the similarity law based on the Zeno line, we

find a critical density of 0.516 g/cm^3 . From the fit to an Antoine law, we obtain the following estimate for the critical pressure $P_c = 886 \text{ bar}$, which is comparable to the results obtained in previous work.²⁹

Focusing now on the case of *Al*, we obtain results for the Boyle parameters that share the same features as for *Be*. The Boyle density we obtain from the EWL simulations (2.56 g/cm^3) is once again in very good agreement with the results from Apfelbaum and Vorob'ev⁸⁰ (2.57 g/cm^3), while we obtain a larger Boyle temperature (with a EWL value of 15316 K compared to 12888 K). For the critical parameters, we have a critical temperature estimated at $T_c = 5412 \text{ K}$, which is approximately a thousand K below the previous estimate $T_c = 6318 \text{ K}$, made on the basis of the liquid data, and a critical density that is larger than the previous estimate (0.45 g/cm^3 versus 0.81 g/cm^3 in this work). The deviation for the critical density can be accounted for the use of a lower value for the critical temperature in the similarity law (Eq. 7). More specifically, the EWL results give a $T_c : T_B$ ratio of 0.35, below the ratio of 0.49 found in previous work,⁸⁰ resulting in a greater value for the $\rho_c : \rho_B$ ratio as fixed by the similarity law. Comparing now our results to those obtained using Gibbs Ensemble Monte Carlo simulations on a different EAM potential¹ and the law of rectilinear diameter, we find that our estimate for the critical density is much closer to that from previous simulation work (0.707 g/cm^3) and that our estimate for the critical temperature is 14% below those results.

In the case of *Cu*, the Boyle parameters we obtain from the EWL simulations on the qSC-EAM potential are in very good agreement with the findings from previous work⁸⁰ both for the Boyle density (8.6 g/cm^3 compared to 8.36 g/cm^3 in this work) and for the Boyle temperature (15593 K compared to 15688 K in this work). In line with the results for *Al*, the EWL critical temperature ($T_c = 5430 \text{ K}$) is below the value extrapolated from the liquid data ($T_c = 7093 \text{ K}$), leading to a larger critical density, since the same similarity law, with different input values for T_c , is used.

We finally compare the critical parameters obtained in this work for *Pb* and *Au* to those estimated from the experimental data on liquid densities by Schroer and Pottlacher,¹⁷ which rely on averaging the results obtained using either 3D-Ising scaling law or a mean-field scaling law. For

Pb, the critical temperature we estimate is $T_c = 2663 \text{ K}$ (as compared to 4636 K in prior work¹⁷), while the critical density we estimate is $\rho_c = 3.54 \text{ g/cm}^3$ is above the critical density from previous work¹⁷ ($\rho_c = 2.322 \text{ g/cm}^3$). For *Au*, we estimate the critical temperature to be $T_c = 4286 \text{ K}$ (as compared to 7217 K in prior work¹⁷) while the critical density we estimate is $\rho_c = 5.96 \text{ g/cm}^3$ is above the critical density from previous work¹⁷ ($\rho_c = 3.544 \text{ g/cm}^3$). The critical temperatures we estimate are therefore below those extrapolated in previous work,¹⁷ while the critical densities we estimate are larger. This is due to two notable differences between the scaling laws used for the critical temperature. First, in our case, we are able to obtain EWL results for high temperature phases and get an accurate estimate for the variations of the density order parameter ($\rho_l - \rho_v$), over a wide temperature range while the extrapolation from the low temperature data only takes into account the variation of ρ_l over a limited temperature range. Second, we use, for the density order parameter, a scaling law with an exponent of 0.326, while the extrapolation from the data¹⁷ calculates the average result for two scaling laws applied to the liquid density ρ_l , one with a 3D-Ising exponent and one with a mean-field exponent of 0.5.

Table 2: Comparison of the critical parameters for selected metals (^a: this work, ^b: Apfelbaum,²⁹ ^c: Apfelbaum and Vorob'ev,⁸⁰ ^d: Schroer and Pottlacher,¹⁷ ^e: Kaptay²⁴ and ^f: Bhatt *et al.* ¹

	T_c (K)	ρ_c (g/cm ³)	P_c (MPa)
<i>Be</i>	4623 ^a	0.52 ^a	88.6 ^a
	5400 ^b	0.26 ^b	46.6 ^b
	10500 ^e		
<i>Al</i>	5412 ^a	0.81 ^a	37.9 ^a
	6378 ^c	0.45 ^c	108.8 ^c
	6299 ^f	0.71 ^f	89.5 ^f
<i>Cu</i>	5430 ^a	3.33 ^a	57.8 ^a
	7093 ^c	1.95 ^c	45.6 ^c
<i>Au</i>	4286 ^a	5.96 ^a	18.6 ^a
	7217 ^d	3.54 ^d	
	8700 ^e		
<i>Pb</i>	2663 ^a	3.54 ^a	7.2 ^a
	4836 ^d	2.32 ^d	
	4200 ^e		

We provide in Fig. 5 a comparison between the EWL result for the vapor pressure and the experimental data. These results show that there is generally a good agreement between the simulation results obtained with the qSC-EAM potential as can be seen most notably in the case of *Ag* and *Cu*. As previously discussed,⁴⁵ the qSC-EAM potential leads to reliable results for the boiling points in most cases (see e.g. *Ag*, *Cu* and *Pt* on the plot), with a few exceptions (e.g. with deviations of up to 10% for *Ni* and *Ir* for the boiling temperatures in Fig. 5).

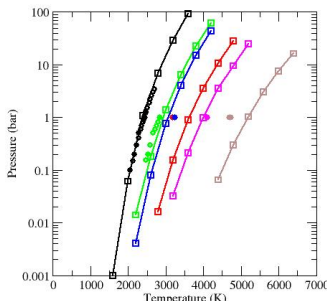


Figure 5: Vapor pressure of selected metals. EWL results are shown as open squares (*Ag* in black, *Cu* in green, *Pd* in blue, *Ni* in red, *Pt* in magenta and *Ir* in brown) while experimental data are shown with open circles⁸¹ and filled circles.⁸²

The EWL results for the variations of the other thermodynamic properties at coexistence are plotted against temperature in Fig. 6. All metals exhibit the same qualitative behavior with the linear variation of μ as a function of T (see bottom of Fig. 6), and the expected decrease of ΔH_{vap} (see top of Fig. 6) and of ΔS_{vap} (see middle of Fig. 6) towards 0 as the temperature approaches the critical temperature. To further analyze the results, we fit the simulation results for the enthalpy of vaporization with the following function:

$$\Delta H_{vap} = A(T_c - T)^a \quad (9)$$

where A and a are two fitting parameters and T_c is the critical temperature previously determined. Carrying out this fit over the set of metals considered here, we find an average critical

exponent for ΔH_{vap} of 0.4. The value for this exponent is very close to the value of 0.38 found in prior work on non-metals.^{83,84} We apply the same analysis to the results for ΔS_{vap} with the following function:

$$\Delta S_{vap} = B(T_c - T)^b \quad (10)$$

where B and b are two fitting parameters and T_c is the critical temperature previously determined. The exponent we find in this case is 1.22. To our knowledge, this provides the first determination, in the case of metals, of the critical exponents for these two scaling laws.

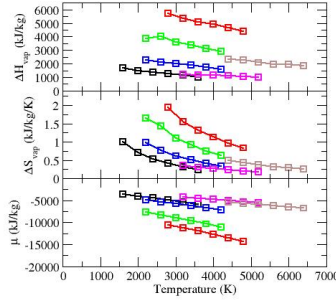


Figure 6: Thermodynamic properties at coexistence for selected metals: ΔH_{vap} against temperature (top), ΔS_{vap} against T (middle) and μ against T (bottom). Same legend as in Fig. 5.

Conclusions

In this work, we carry out EWL simulations to determine the binodal and the Zeno line of 11 FCC and HCP metals (*Ag, Al, Au, Be, Cu, Ir, Ni, Pb, Pd, Pt* and *Rh*), modeled with a many-body potential known as the qSC-EAM model. We estimate the critical parameters according to a three-step procedure with (i) the calculation of the critical temperature from a scaling law for the density (with a critical exponent of 0.326), (ii) the determination of the critical density using a similarity law and the Boyle parameters defining the Zeno line, and (iii) the evaluation of

the critical pressure from an Antoine law fitted to the simulation results for the vapor pressure. We compare our results to estimates made in prior work on the basis of the experimental data for liquid densities and, when available, to previous simulation work that relied on the law of rectilinear diameters. The results obtained with our EWL simulations cover a wider range of temperatures than that covered in the extrapolations from the liquid densities data. They also take into account the variations of the density order parameter ($\rho_l - \rho_v$) at high temperature, which are not included when the extrapolation from low temperature liquid data only is carried out. Applying the three-step procedure to the 11 *FCC* and *HCP* metals studied in this work allows us to provide an estimate for the critical parameters for all systems. These estimates generally lead to lower critical temperatures and, as a result, to larger critical densities than those obtained from extrapolations relying on low temperature liquid data only. Our results also allow us to propose two scaling laws for the enthalpy of vaporization and the entropy of vaporization with the corresponding critical exponents of 0.4 and 1.22 respectively. Further work testing the validity of these two scaling laws on other systems is currently under way.

Acknowledgement

Partial funding for this research was provided by NSF through CAREER award DMR-1052808.

References

- (1) Bhatt, D.; Jasper, A. W.; Schultz, N. E.; Siepmann, J. I.; Truhlar, D. G. Critical properties of aluminum. *J. Am. Chem. Soc.* **2006**, *128*, 4224–4225.
- (2) Rowlinson, J. S.; Swinton, F. L. *Liquids and Liquid Mixtures*; Butterworths, London, 1982.
- (3) Delhommelle, J.; Boutin, A.; Tavitian, B.; Mackie, A. D.; Fuchs, A. H. Vapour-liquid coexistence curves of the united-atom and anisotropic united-atom force fields for alkane mixtures. *Mol. Phys.* **1999**, *96*, 1517–1524.

- (4) Potoff, J.; Errington, J.; Panagiotopoulos, A. Molecular simulation of phase equilibria for mixtures of polar and non-polar components. *Mol. Phys.* **1999**, *97*, 1073–1083.
- (5) Errington, J. R.; Boulougouris, G. C.; Economou, I. G.; Panagiotopoulos, A. Z.; Theodorou, D. N. Molecular simulation of phase equilibria for water-methane and water-ethane mixtures. *J. Phys. Chem. B* **1998**, *102*, 8865–8873.
- (6) Messerly, R. A.; Rowley, R. L.; Knotts IV, T. A.; Wilding, W. V. An improved statistical analysis for predicting the critical temperature and critical density with Gibbs ensemble Monte Carlo simulation. *J. Chem. Phys.* **2015**, *143*, 104101.
- (7) Schnabel, T.; Vrabec, J.; Hasse, H. Unlike Lennard–Jones parameters for vapor–liquid equilibria. *J. Mol. Liq.* **2007**, *135*, 170–178.
- (8) Panagiotopoulos, A. Z. Direct determination of phase coexistence properties of fluids by Monte Carlo simulation in a new ensemble. *Mol. Phys.* **1987**, *61*, 813–826.
- (9) Cailletet, L.; Mathias, E. *C.R Acad. Sci.* **1886**, *102*, 1202.
- (10) Widom, B.; Rowlinson, J. S. New model for the study of liquid–vapor phase transitions. *J. Chem. Phys.* **1970**, *52*, 1670–1684.
- (11) Narger, U.; Balzarini, D. A. Coexistence-curve diameter and critical density of xenon. *Phys. Rev. B* **1990**, *42*, 6651–6657.
- (12) Weiner, J.; Langley, K. H.; Ford, N. C. Experimental Evidence for a Departure from the Law of the Rectilinear Diameter. *Phys. Rev. Lett.* **1974**, *32*, 879–881.
- (13) Fisher, M. E.; Orkoulas, G. The Yang-Yang Anomaly in Fluid Criticality: Experiment and Scaling Theory. *Phys. Rev. Lett.* **2000**, *85*, 696–699.
- (14) Sengers, J. V.; Shanks, J. G. Experimental critical-exponent values for fluids. *J. Stat. Phys.* **2009**, *137*, 857–877.

- (15) Jüngst, S.; Knuth, B.; Hensel, F. Observation of singular diameters in the coexistence curves of metals. *Phys. Rev. Lett.* **1985**, *55*, 2160.
- (16) Goldstein, R. E.; Ashcroft, N. W. Origin of the Singular Diameter in the Coexistence Curve of a Metal. *Phys. Rev. Lett.* **1985**, *55*, 2164.
- (17) Schröer, W.; Pottlacher, G. Estimation of critical data and phase diagrams of pure molten metals. *High Temperatures–High Pressures* **2014**, *43*.
- (18) Goldstein, R. E.; Parola, A.; Ashcroft, N.; Pestak, M.; Chan, M.; de Bruyn, J. R.; Balzarini, D. Beyond the pair-potential model of fluids at the liquid-vapor critical point. *Phys. Rev. Lett.* **1987**, *58*, 41.
- (19) Bhatt, D.; Schultz, N. E.; Jasper, A. W.; Siepmann, J. I.; Truhlar, D. G. Phase behavior of elemental aluminum using Monte Carlo simulations. *J. Phys. Chem. B* **2006**, *110*, 26135–26142.
- (20) Pottlacher, G.; Jäger, H. A review of determinations of critical point data of metals using subsecond pulse heating techniques. *J. Non-Cryst. Solids* **1996**, *205*, 265–269.
- (21) Pottlacher, G.; Kaschnitz, E.; Jäger, H. Investigations of thermophysical properties of liquid metals with a rapid resistive heating technique. *J. Non-Cryst. Solids* **1993**, *156*, 374–378.
- (22) Lang, G. *IMetallkunde* **2012**, *68*, 213.
- (23) Chhabra, R. Surface tension of liquid metals: a predictive approach. *High Temp. High Press.* **1990**, *22*, 171–175.
- (24) Kaptay, G. On the Order–Disorder Surface Phase Transition and Critical Temperature of Pure Metals Originating from BCC, FCC, and HCP Crystal Structures. *Int. J. Thermophys.* **2012**, *33*, 1177–1190.
- (25) Morel, V.; Bultel, A.; Chéron, B. The critical temperature of aluminum. *Int. J. Thermophys.* **2009**, *30*, 1853–1863.

- (26) Ramana, A. S. V. Molecular dynamics simulation of liquid–vapor phase diagrams of metals modeled using modified empirical pair potentials. *Fluid Phase Equil.* **2014**, *361*, 181–187.
- (27) Singh, J. K.; Adhikari, J.; Kwak, S. K. Vapor–liquid phase coexistence curves for Morse fluids. *Fluid Phase Equil.* **2006**, *248*, 1–6.
- (28) Apfelbaum, E. M.; Vorob'ev, V. S. The Wide-Range Method to Construct the Entire Coexistence Liquid–Gas Curve and to Determine the Critical Parameters of Metals. *J. Phys. Chem. B* **2015**, *119*, 11825–11832.
- (29) Apfelbaum, E. Estimate of Beryllium Critical Point on the Basis of Correspondence between the Critical and the Zeno-Line Parameters. *J. Phys. Chem. B* **2012**, *116*, 14660–14666.
- (30) Apfelbaum, E.; Vorob'ev, V. The saturation pressure for different objects in reduced variables and the justification of some empirical relations set from the van der Waals equation. *Chem. Phys. Lett.* **2014**, *591*, 212–215.
- (31) Apfelbaum, E.; Vorob'ev, V. A new similarity found from the correspondence of the critical and Zeno-line parameters. *J. Phys. Chem. B* **2008**, *112*, 13064–13069.
- (32) Apfelbaum, E.; Vorob'ev, V.; Martynov, G. Triangle of liquid-gas states. *J. Phys. Chem. B* **2006**, *110*, 8474–8480.
- (33) Kulinskii, V. Simple geometrical interpretation of the linear character for the Zeno-line and the rectilinear diameter. *J. Phys. Chem. B* **2010**, *114*, 2852–2855.
- (34) Kulinskii, V. The critical compressibility factor value: Associative fluids and liquid alkali metals. *J. Chem. Phys.* **2014**, *141*, 054503.
- (35) Vorob'ev, V. How to turn real substance liquid–gas coexistence curve in binodal of lattice gas. *Chem. Phys. Lett.* **2014**, *605*, 47–50.

- (36) Luo, S.-N.; Ahrens, T. J.; Çağın, T.; Strachan, A.; Goddard III, W. A.; Swift, D. C. Maximum superheating and undercooling: Systematics, molecular dynamics simulations, and dynamic experiments. *Phys. Rev. B* **2003**, *68*, 134206.
- (37) Kart, H.; Tomak, M.; Uludoğan, M.; Çağın, T. Thermodynamical and mechanical properties of Pd–Ag alloys. *Comput. Mat. Sci.* **2005**, *32*, 107–117.
- (38) Xu, P.; Cagin, T.; Goddard III, W. A. Assessment of phenomenological models for viscosity of liquids based on nonequilibrium atomistic simulations of copper. *J. Chem. Phys.* **2005**, *123*, 104506.
- (39) Qi, Y.; Çağın, T.; Kimura, Y.; Goddard Iii, W. A. Viscosities of liquid metal alloys from nonequilibrium molecular dynamics. *Journal of computer-aided materials design* **2001**, *8*, 233–243.
- (40) Kart, S. Ö.; Tomak, M.; Uludoğan, M.; Çağın, T. Liquid properties of Pd–Ni alloys. *J. Non-Cryst. Solids* **2004**, *337*, 101–108.
- (41) Kart, S. Ö.; Tomak, M.; Uludoğan, M.; Çağın, T. Structural, thermodynamical, and transport properties of undercooled binary Pd–Ni alloys. *Mat. Sci. Eng. A* **2006**, *435*, 736–744.
- (42) Desgranges, C.; Delhommelle, J. Viscosity of liquid iron under high pressure and high temperature: Equilibrium and nonequilibrium molecular dynamics simulation studies. *Phys. Rev. B* **2007**, *76*, 172102.
- (43) Desgranges, C.; Delhommelle, J. Shear viscosity of liquid copper at experimentally accessible shear rates: Application of the transient-time correlation function formalism. *J. Chem. Phys.* **2008**, *128*, 084506.
- (44) Desgranges, C.; Delhommelle, J. Rheology of liquid fcc metals: Equilibrium and transient-time correlation-function nonequilibrium molecular dynamics simulations. *Phys. Rev. B* **2008**, *78*, 184202.

- (45) Gelb, L. D.; Chakraborty, S. N. Boiling point determination using adiabatic Gibbs ensemble Monte Carlo simulations: Application to metals described by embedded-atom potentials. *J. Chem. Phys.* **2011**, *135*, 224113.
- (46) Desgranges, C.; Kastl, E. A.; Aleksandrov, T.; Delhommelle, J. Optimisation of Multiple Time-Step Hybrid Monte Carlo Wang–Landau Simulations in the Isobaric–Isothermal Ensemble for the Determination of Phase Equilibria. *Molec. Simul.* **2010**, *36*, 544–551.
- (47) Aleksandrov, T.; Desgranges, C.; Delhommelle, J. Numerical Estimate for Boiling Points via Wang-Landau Simulations. *Molec. Simul.* **2012**, *38*, 1265–1270.
- (48) Desgranges, C.; Delhommelle, J. Evaluation of the Grand-Canonical Partition Function using Expanded Wang-Landau Simulations. I. Thermodynamic Properties in the Bulk and at the Liquid-Vapor Phase Boundary. *J. Chem. Phys.* **2012**, *136*, 184107.
- (49) Desgranges, C.; Delhommelle, J. Evaluation of the Grand-Canonical Partition Function using Expanded Wang-Landau Simulations. II. Adsorption of Atomic and Molecular Fluids in a Porous Material. *J. Chem. Phys.* **2012**, *136*, 184108.
- (50) Desgranges, C.; Delhommelle, J. Evaluation of the Grand-Canonical Partition Function using Expanded Wang-Landau Simulations. III. Adsorption of Atomic and Molecular Fluids in a Porous Material. *J. Chem. Phys.* **2012**, *136*, 184108.
- (51) Desgranges, C.; Delhommelle, J. Evaluation of the grand-canonical partition function using expanded Wang-Landau simulations. IV. Performance of many-body force fields and tight-binding schemes for the fluid phases of silicon. *J. Chem. Phys.* **2016**, *144*, 124510.
- (52) Wang, F.; Landau, D. P. Determining the Density of States for Classical Statistical Models: A Random Walk Algorithm to produce a Flat Histogram. *Phys. Rev. E* **2001**, *64*, 056101.
- (53) Wang, F.; Landau, D. Efficient, Multiple-Range Random Walk Algorithm to calculate the Density of States. *Phys. Rev. Lett.* **2001**, *86*, 2050–2053.

- (54) Shell, M. S.; Debenedetti, P. G.; Panagiotopoulos, A. Z. Generalization of the Wang-Landau Method for Off-Lattice Simulations. *Phys. Rev. E* **2002**, *66*, 056703.
- (55) Yan, Q.; Faller, R.; de Pablo, J. J. Density-of-States Monte Carlo Method for Simulation of Fluids. *J. Chem. Phys.* **2002**, *116*, 8745–8750.
- (56) Gazenmüller, G.; Camp, P. J. Applications of Wang-Landau Sampling to Determine Phase Equilibria in Complex Fluids. *J. Chem. Phys.* **2007**, *127*, 154504.
- (57) Desgranges, C.; Delhommelle, J. Phase Equilibria of Molecular Fluids via Hybrid Monte Carlo Wang-Landau Simulations: Applications to Benzene and n-Alkanes. *J. Chem. Phys.* **2009**, *130*, 244109.
- (58) Desgranges, C.; Hicks, J. M.; Magness, A.; Delhommelle, J. Phase Equilibria of Polyaromatic Hydrocarbons by Hybrid Monte Carlo Wang–Landau Simulations. *Mol. Phys.* **2010**, *108*, 151–158.
- (59) Ngale, K. N.; Desgranges, C.; Delhommelle, J. Wang-Landau Configurational Bias Monte Carlo Simulations: Vapour-Liquid Equilibria of Alkenes. *Molec. Simul.* **2012**, *38*, 653–658.
- (60) Desgranges, C.; Ngale, K.; Delhommelle, J. Prediction of Critical Properties for Naphthalene, Triphenylene and Chrysene by Wang-Landau Simulations. *Fluid Phase Equil.* **2012**, *322-323*, 92–96.
- (61) Escobedo, F.; de Pablo, J. J. Expanded Grand Canonical and Gibbs Ensemble Monte Carlo Simulation of Polymers. *J. Chem. Phys.* **1996**, *105*, 4391.
- (62) Lyubartsev, A. P.; Martsinovski, A. A.; Shevkunov, S. V.; Vorontsov-Velyaminov, P. N. New Approach to Monte Carlo Calculation of the Free Energy: Method of Expanded Ensembles. *J. Chem. Phys.* **1992**, *96*, 1776–1783.
- (63) Muller, M.; Paul, W. Measuring the Chemical Potential of Polymer Solutions and Melts in Computer Simulations. *J. Chem. Phys.* **1994**, *100*, 719–724.

- (64) Shi, W.; Maginn, E. J. Continuous Fractional Component Monte Carlo: An Adaptive Biasing Method for Open System Atomistic Simulations. *J. Chem. Theory Comp.* **2007**, *3*, 1451–1463.
- (65) Singh, J. K.; Errington, J. R. Calculation of Phase Coexistence Properties and Surface Tensions of n-Alkanes with Grand-Canonical Transition-Matrix Monte Carlo Simulation and Finite-Size Scaling. *J. Phys. Chem. B* **2006**, *110*, 1369–1376.
- (66) Escobedo, F. A.; Martinez-Veracoechea, F. J. Optimized Expanded Ensembles for Simulations involving Molecular Insertions and Deletions. I. Closed systems. *J. Chem. Phys.* **2007**, *127*, 174103.
- (67) Escobedo, F. A.; Martinez-Veracoechea, F. J. Optimization of Expanded Ensemble Methods. *J. Chem. Phys.* **2008**, *129*, 154107.
- (68) Rane, K. S.; Murali, S.; Errington, J. R. Monte Carlo Simulation Methods for Computing Liquid–Vapor Saturation Properties of Model Systems. *J. Chem. Theory Comput.* **2013**, *9*, 2552–2566.
- (69) Rane, K. S.; Errington, J. R. Using Monte Carlo Simulation to Compute Liquid–Vapor Saturation Properties of Ionic Liquids. *J. Phys. Chem. B* **2013**, *117*, 8018–8030.
- (70) Koenig, A. R. V.; Desgranges, C.; Delhommelle, J. Adsorption of Hydrogen in Covalent Organic Frameworks using Expanded Wang–Landau Simulations. *Molec. Simul.* **2014**, *40*, 71–79.
- (71) Hicks, E. A.; Desgranges, C.; Delhommelle, J. Adsorption and Diffusion of the Antiparkinsonian Drug Amantadine in Carbon Nanotubes. *Molec. Simul.* **2014**, *40*, 656–663.
- (72) Owen, A. N.; Desgranges, C.; Delhommelle, J. A new force field for H_2S and its binary and ternary mixtures with CO_2 and CH_4 . *Fluid Phase Equil.* **2015**, *402*, 69–77.

- (73) Desgranges, C.; Delhommelle, J. Many-body effects on the thermodynamics of fluids, mixtures and nanoconfined fluids. *J. Chem. Theory Comput.* **2015**, *11*, 5401.
- (74) McQuarrie, D. A. *Statistical Mechanics*; Harper & Row, New York, 1976.
- (75) Finnis, M.; Sinclair, J. A simple empirical N-body potential for transition metals. *Phil. Mag. A* **1984**, *50*, 45–55.
- (76) Sutton, A.; Chen, J. Long-range finnis–sinclair potentials. *Phil. Mag. Lett.* **1990**, *61*, 139–146.
- (77) Mei, J.; Davenport, J.; Fernando, G. Analytic embedded-atom potentials for fcc metals: Application to liquid and solid copper. *Phys. Rev. B* **1991**, *43*, 4653.
- (78) Daw, M. S.; Baskes, M. I. Semiempirical, quantum mechanical calculation of hydrogen embrittlement in metals. *Phys. Rev. Lett.* **1983**, *50*, 1285.
- (79) Fokin, L. R.; Popov, V. N. General function of the unit compressibility factor for liquid and gaseous mercury. *High Temperature* **2013**, *51*, 465–468.
- (80) Apfelbaum, E.; Vorob'ev, V. The predictions of the critical point parameters for Al, Cu and W found from the correspondence between the critical point and unit compressibility line (Zeno line) positions. *Chem. Phys. Lett.* **2009**, *467*, 318–322.
- (81) Geiger, F.; Busse, C.; Loehrke, R. The vapor pressure of indium, silver, gallium, copper, tin, and gold between 0.1 and 3.0 bar. *Int. J. Thermophys.* **1987**, *8*, 425–436.
- (82) Linde, D. *Handbook of Chemistry and Physics*. CRC Press. *Boca Raton* **1994**,
- (83) Watson, K. Thermodynamics of the liquid state. *Ind. Eng. Chem.* **1943**, *35*, 398–406.
- (84) Leibovici, C. F.; Nichita, D. V. New basis functions for the representation of vapor pressure data. *Fluid Phase Equil.* **2014**, *361*, 1–15.

Graphical Abstract

